Industrial Crops & Products 235 (2025) 121814

Contents lists available at ScienceDirect

Industrial Crops & Products

journal homepage: www.elsevier.com/locate/indcrop

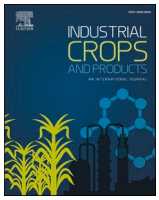

Integrating biofumigation and phyto-spectral monitoring: Advancing sustainable agricultural practices

Juan Manuel Arroyo, Jose Soler, Rubén Linares, Lorena Parra, Daniel Palmero *

Departmento de Producción Agraria, Escuela Técnica Superior de Ingeniería Agronómica, Alimentaria y de Biosistemas, Universidad Politécnica de Madrid, Avenida Puerta de Hierro, 4, Madrid 28040, Spain

ARTICLE INFO

Keywords:
Brassicaceae
Vegetation Indices
Glucosinolates
Above-ground biomass
Agroecology
Machine learning

ABSTRACT

Biofumigation is a sustainable agricultural practice that utilizes the biocidal properties of natural compounds, such as isothiocyanates (ITCs) derived from glucosinolates (GSLs), to control soilborne pathogens and improve soil health. This study evaluates the biofumigant potential of various Brassicaceae species, emphasizing their biomass production, GSLs concentrations, and their utility in sustainable soil management under frost-prone conditions in central Spain over two different growing seasons. Additionally, phyto-spectral indices derived from remote sensing technologies, including Normalized Difference Vegetation Index (NDVI), Green Normalized Difference Vegetation Index (GNDVI), Normalized Difference Red Edge (NDRE), and Transformed Chlorophyll Absorption in Reflectance Index/Optimized Soil Adjusted Vegetation Index (TCARI/OSAVI), were obtained along six flights. Data have been analyzed to optimize the timing of biofumigant incorporation into the soil and assess their correlation with biomass and GSLs content. The findings identify *Brassica juncea* and *B. carinata* as the most effective biofumigant species due to their high aliphatic glucosinolate content. In contrast, *B. napus* showed superior frost tolerance. Vegetation indices demonstrated strong relationships with biomass and GSLs content during key growth stages, with NDRE showing especially good performance under certain developmental conditions. While, regression models obtained with machine learning tools enhanced the predictive accuracy for biomass and GSLs concentrations for the entire growing period, demonstrating their potential for integrating precision agriculture tools into biofumigation practices. This study advances the understanding of biofumigant crop management by incorporating spectral technologies to enhance efficiency and decision-making, aligning with sustainable agriculture and precision farming principles.

1. Introduction

In response to environmental challenges and increasingly strict regulations on chemical fumigants, biofumigation has emerged as a viable alternative to improve soil health and promote environmental friendly agricultural practices. Biofumigation is an agroecological technique that leverages the biocidal properties of natural compounds to control pathogens and improve soil health (Kirkegaard et al., 1993). This process involves the incorporation of plant biomass into the soil, where tissue decomposition releases chemical compounds like isothiocyanates, which are highly effective in suppressing harmful microorganisms (dos Santos et al., 2021; Morris et al., 2020). Furthermore, biofumigant species also function as cover crops, providing soil protection against erosion, maintaining organic matter balance, improving soil structure, and reducing nutrient leaching, particularly nitrogen (Brennan et al., 2020; Clarkson et al., 2015; Haramoto and Gallandt, 2004). These agricultural practices align perfectly with the new environmental strategies, such as the "Farm to Fork Strategy" (Arroyo et al., 2025).

Among the species used for biofumigation, those in the Brassicaceae family stand out for their efficacy. These plants are characterized by their rapid growth, high biomass production (Brant et al., 2011; Elhakeem et al., 2021), and synthesis of elevated levels of glucosinolates (GLS), which are secondary compounds with biocidal properties. These GSLs, primarily found in the genera *Brassica*, *Raphanus*, *Sinapis*, and *Eruca*, are metabolites that decompose into isothiocyanates (ITCs) through the action of the enzyme myrosinase (Agerbirk and Olsen, 2012; Fahey et al., 2001; Gimsing and Kirkegaard, 2009; Morris et al., 2020; Wieczorek et al., 2024). ITCs, known for their broad-spectrum antimicrobial activity, are effective in controlling soilborne diseases (Agerbirk and Olsen, 2012; Björkman et al., 2011; Gimsing and Kirkegaard, 2009;

* Corresponding author.
E-mail address: daniel.palmero@upm.es (D. Palmero).

https://doi.org/10.1016/j.indcrop.2025.121814
Received 15 March 2025; Received in revised form 26 August 2025; Accepted 26 August 2025
Available online 30 August 2025

Matthiessen and Kirkegaard, 2006). While other compounds like nitriles and sulfides are also generated, their contribution to the biofumigation effect is less significant than that of ITCs (Agerbirk and Olsen, 2012; Gimsing and Kirkegaard, 2009). Generally, the highest GSLs concentrations are found in seeds, followed by aerial and underground tissues (Bellostas et al., 2007; Fourie et al., 2016; Morris et al., 2020). Although GSLs concentrations in plant tissues are genetically determined, their levels also depend on other factors, such as the developmental stage of each species and environmental conditions (e.g., drought, sulphur and nitrogen availability, season, and diurnal cycle) (Bellostas et al., 2004; Ben Ammar et al., 2023; Fourie et al., 2016; Kirkegaard and Sarwar, 1998; Morris et al., 2020).

Previous studies (Sarwar and Kirkegaard, 1998) showed that the total GSL concentration in eight Brassicaceae species generally declined from the bud stage to flowering under different environmental conditions, reaching the lowest levels at maturity—except in plants grown in a glasshouse, where most species exhibited an increase in GSL concentration at flowering.

Similarly, *Brassica nigra* and *B. juncea* cultivated in glasshouse conditions had the highest GSL concentrations at the final growth stage (when seeds in the lower pods reached full size), whereas *B. carinata* and *B. rapa* showed the highest concentrations at early growth stages (from four-leaf stage to pedicel elongation, (Bellostas et al., 2004)). These findings indicate that the dynamics of GSL accumulation in Brassica tissues are species-specific and strongly influenced by environmental conditions.

Despite the observed variations in GSL concentration across developmental stages, the highest biofumigation potential of the studied species generally occurred at the final growth stage due to greater biomass accumulation compared with earlier stages (Bellostas et al., 2004; Kirkegaard and Sarwar, 1998).

Nonetheless, GSL tissue concentration and biomass accumulation are not the only factors to be considered since the GSL profile and selection of species adapted to specific climatic conditions and crop cycles also play an important role in biofumigation efficacy (Arroyo et al., 2025).

In this context, emerging technologies such as phyto-spectral vegetation indices derived from remote sensors have opened new possibilities for detecting and mapping crop status in large areas, optimizing these sustainable practices (Gabbrielli et al., 2022). Vegetation indices are algebraic combinations of two or more values of reflectance measured in specific regions of the electromagnetic spectrum (Gabbrielli et al., 2022). Many researchers have shown that vegetation indices are essential tools in precision agriculture, demonstrating their utility in predicting crop biomass and yield, monitoring growth status, and detecting specific crop stressors for field crops like rapeseed (Gabbrielli et al., 2022; Liu et al., 2019; Zamani-Noor and Feistkorn, 2022). Technologies like unmanned aerial vehicles (UAV) equipped with high multispectral resolution cameras allow accurate detection of the spatial unevenness of plant stands, which is the basis for targeted and efficient measures in line with the principles of precision agriculture (Lukas et al., 2022). Nonetheless, only a few studies have shown that optical reflectance spectroscopy is a potential tool for the estimation of GSL content in Brassicaceae. In the last few years, different researchers have found that spectral reflectance in several wavelength bands between 385, 860 and 1000 nm was correlated to individual GSLs content in the leaf of Brassica rapa and Brassica oleracea (Chowdhury et al., 2021; Ngo et al., 2019). Related to these researches, Soengas et al., (2023) found that populations of Brassica oleracea with high indolic glucobrassicin content showed lower NDVI values than populations with low content of this GSL. In addition to these tools, some authors have shown that absorbance measures at 650 nm (red) and 940 nm (NIR) are valuable for determining GSLs content. For example, Arroyo et al., (2025) found a correlation between Chlorophyll Content Index (SPAD) and GSLs concentration in the biomass of different biofumigant Brassicaceae species. Meanwhile, Mawlong et al., (2017) showed that absorbance at 425 nm is correlated to total GSLs content in the defatted seed meal of Brassica napus.

The aim of the paper is to complement the previous advancements in biofumigation by incorporating phyto-spectral indices and Machine-Learning (ML) techniques as tools for the efficient monitoring and management of biofumigant crops. The paper is based on data from five Brassicaceae species in two different growing seasons. First, we characterize total dry biomass production and its distribution between above-ground and root dry biomass, and we establish correlations with GSLs concentrations in the biomass according to the vegetation indices. These vegetation indices include NDVI, GNDVI, TCARI/OSAVI, and NDRE, obtained through a UAV equipped with a multispectral camera. This approach represents a significant advancement in identifying the optimal timing for residue incorporation into the soil. It not only enhances knowledge about biofumigation but also facilitates the integration of precision agriculture into sustainable farming and agroecological practices.

2. Materials and methods

2.1. Location and soil and climatic conditions

The trial was carried out at the Experimental Fields of School of Agricultural, Food, and Biosystems Engineering, Universidad Politécnica de Madrid (UPM), during the 2022–2023 and 2024–2025 agricultural seasons. This region is located in Madrid, in the centre of the Iberian Peninsula (40°26 N; 3°44 W and 600 m above sea level). The soil in the experimental plot had a sandy loam texture, with a basic pH ranging from 7.8 to 8.2 and a low organic matter content (1–1.2 %). The carbon/nitrogen ratio was 8, and the electrical conductivity measured in a 1:5 extract ranged from 0.12 to 0.16 dS/m. Based on analyses conducted on four soil samples, one from each trial block, taken from the 0–30 cm and 30–60 cm layers, high concentrations of calcium (≥2500 mg/kg), magnesium (≥250 mg/kg), potassium (≥300 mg/kg), and phosphorus (≥25 mg/kg) were recorded. Weather conditions for the 2022–2023 growing season included a notably dry autumn and a cold winter, marked by an extended frost period, see Fig. 1a). During 2024–2025, the climatic conditions changed: wet October and dry and frost December (Fig. 1b).

2.2. Experimental design

The experiment followed a randomized complete block design with four replicates. The primary factor was the biofumigant species. Five species were evaluated: Brassica carinata A.Braun., (cv. Eleven), Brassica juncea (L.) Vassiliĭ Matveievitch Czernajew., (cv. Scala), Brassica napus L., (cv. Gordon), Raphanus sativus L., (cv. Córdoba), and Sinapis alba L., (cv. Venice). Each elementary plot measured 10 m in length and 3.6 m in width, totalling 36 m^2 per plot.

Sowing was carried out on September 22, 2022 and September 18, 2024, using an experimental seeder with a working width of 1.2 m. Seeding rates were 12.5 kg/ha for B. carinata, B. napus, and B. juncea and 25 kg/ha for R. sativus and S. alba. Two post-sowing irrigations of 15 mm each were applied in late September and early October to ensure germination. Fertilization was achieved with 400 kg/ha of a compound N-P-K(S) 15–15–15 (13) fertilizer applied pre-sowing.

2.3. Analytical determinations

Biomass production was quantified for above-ground at various growth stages. Sampling was conducted in a 0.5 m^2 area (1 m × 0.5 m) within each plot on January 23 and March 27, 2023 (123 and 186 days after sowing, respectively). Total fresh biomass weights were recorded from each area plot. Three subsamples of representative plants from each area plot were then selected, and dry matter biomass was determined by drying in a forced-air oven at 65 °C until constant weight. Values for total above-ground dry biomass (AGB) were calculated using

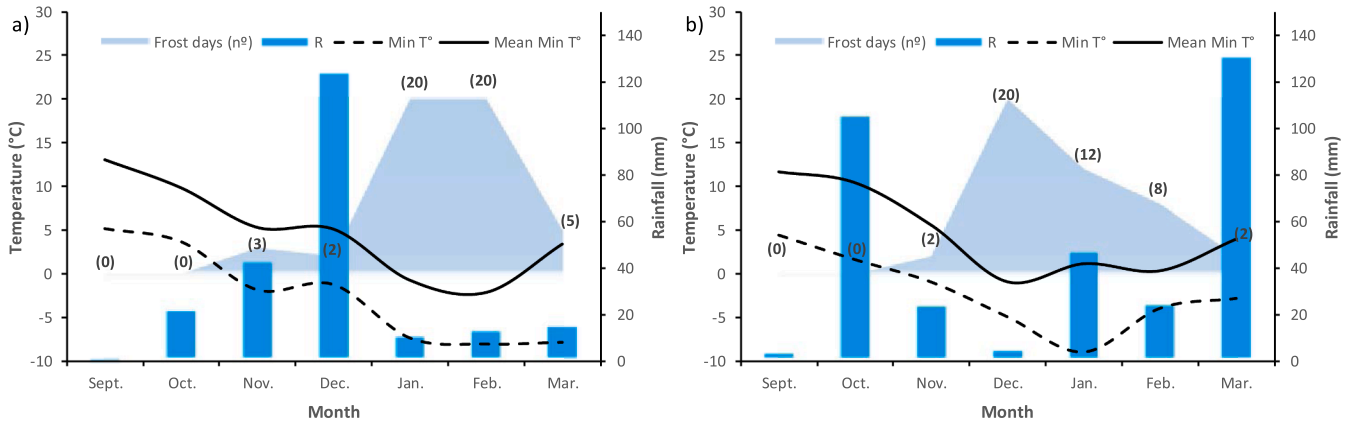

Fig. 1. Weather data during a) the 2022–2023 and b) 2024–2025 growing season. Frost days represent the number of days per month when the minimum temperature was below 0 °C; R: rainfall; Min T°: minimum temperature; and Mean Min T°: mean minimum temperature.

their respective fresh biomass/dry biomass ratio.

The GSLs were extracted, purified, desulfated, and analyzed following the ISO, (9167)–1, protocol (1992) with modifications. Briefly, 50 mg of powdered plant material was placed in test tubes, and 1.5 ML of 70 % methanol and 100 μL of glucotropaeolin (internal standard) was added. The mixture was incubated at 80 °C for extraction, centrifuged, and the supernatant was used for further analysis. Purification was carried out using 96-well plates loaded with ion-exchange resin and desulfation using sulfatase. Desulfoglucosinolates were quantified by high-performance liquid chromatography equipped with an ultraviolet detector set at 229 Palatino LinotypeMultispectral images were captured by a 3D Robotics Iris + equipped with handheld monitors at four different stages of the Brassicaceae cycle using a MicaSense RedEdge-MX camera. Flights were conducted using a predefined path, and images with 1280 × 1024 resolution were processed to calculate vegetation indices for each plot. These indices include the Normalized Difference Vegetation Index (NDVI) (Rouse et al., 1974), Green Normalized Difference Vegetation Index (GNDVI) (Gitelson et al., 1995), Normalized Difference Red Edge Index (NDRE) (Tucker, 1979 Palatino Linotype Haboudane et al., 2002), and Optimized Soil-Adjusted Vegetation Index (OSAVI) (Rondeaux et al., 1996).

Eq. (1): Normalized Difference Vegetation Index (NDVI)

$$NDVI = \frac{R_{800} - R_{670}}{R_{800} + R_{670}}$$

Eq. (2): Green Normalized Difference Vegetation Index (GNDVI)

$$GNDVI = \frac{R_{800} - R_{550}}{R_{800} + R_{550}}$$

Eq. (3): Normalized Difference Red Edge (NDRE)

$$NDRE = \frac{R_{800} - R_{740}}{R_{800} + R_{740}}$$

Eq. (4): Transformed Chlorophyll Absorption in Reflectance Index (TCARI)

$$TCARI = 3 \times \left[(R_{700} - R_{670}) - \frac{2 \times (R_{700} - R_{550})}{\frac{R_{700}}{R_{670}}} \right]$$

Eq. (5): Optimized Soil-Adjusted Vegetation Index (OSAVI)

$$OSAVI = 1.16 \times \frac{R_{800} - R_{670}}{R_{800} + R_{670} + 0.16}$$

Where R(x) represents the reflectance of the vegetation cover in the electromagnetic spectrum band corresponding to a wavelength of "x" nm. Each vegetation index was calculated according to its respective formula (Eqs. (1)–(5)).

2.4. Statistical analysis

An analysis of variance (ANOVA) was performed for biomass, GSL concentrations, and vegetation indices. Fisher's LSD test at 95 % confidence was used for mean separation. Relationships between parameters were analyzed using both linear and non-linear regression models, including second-order polynomial and exponential fits. Model selection was based on the highest coefficient of determination (R^2) and the lowest root mean square error (RMSE). The statistical analyses were performed using STATGRAPHICS Centurion XVIII (StatPoint, Inc., Herndon, VA, USA).

2.5. Regression models and MATLAB regression learner for predicting biomass and GSL concentrations

The data gathered during drone flights from the multiple indices and the data obtained through chemical analyses at the laboratory have been combined to build the dataset for the paper for predicting biomass and GSL concentrations. The dataset includes 72 samples collected over two experimental periods. Vegetation index values, species code, and biomass were recorded for all samples, while GSL concentrations were determined in a representative subset of 60 samples.

Initially, Simple Regression (SR) analyses were performed using individual indices, and Multiple Regression (MR) analyses were conducted incorporating all indices along with the species code. These analyses were carried out using the STATGRAPHICS Centurion XVIII statistical software package (StatPoint, Inc., Herndon, VA, USA). Both SR and MR models were fitted using the entire dataset, and the resulting metrics included the coefficient of determination (R^2) and the associated p-values.

Subsequently, regression analyses were performed using the Regression Learner (RL) from the machine learning toolset in MATLAB R2025a (MathWorks, Natick, MA, USA), following two different approaches. First, models were trained using each vegetation index individually in combination with the species code. Second, a multiple regression model was developed incorporating all indices and species codes. For RL analyses, the dataset was divided into training and testing subsets: the first, second, and fourth field replicates were used for training (n = 40, representing 67 % of the dataset), while the third replicate served as the test set (n = 20, 33 % of the dataset).

Given the limited number of samples, cross-fold techniques have been used. Particularly, 10 folds are generated with the dataset to train and validate the obtained models. The dataset was split into training and

test subsets: the first, second, and fourth replicates of the field trials were used as the training dataset (40 out of 60 samples, 66 % of the original dataset), while the third replicate was used as the test dataset (20 samples, 33 %). The models used include discriminant analysis, naive Bayes, trees, support vector machines, K-nearest neighbours, and neural networks, resulting in 28 different regressions for each analysed parameter. For SR and MR metrics, the models include R^2 for the training and test dataset.

3. Results and discussion

3.1. Phyto-spectral indices

This subsection analyses the relationship between spectral indices and their ability to differentiate biofumigant species. Before describing in detail the results, Tables 1 and 2 provide an overview of the index values obtained across the two growing seasons (2022–2023 and 2024–2025, respectively). The statistical significance from the ANOVA tests has been added to the obtained values. The five species included in the trials—Brassica carinata, B. juncea, B. napus, Raphanus sativus, and Sinapis alba—showed consistent differences in spectral response across sampling dates and vegetation indices.

Table 1
Vegetation indices values for biofumigant species across different sampling dates during the first cycle.

Sampling date and index	Species					
	B. carinata	*B. juncea*	*B. napus*	*R. sativus*	*S. alba*	***p* value**
29/10/2022 (37 DAS[1])						
NDVI[2]	0.826c[6]	0.822c	0.849 b	0.858 ab	0.875 a	***[7]
GNDVI[3]	2.775 b	2.755 b	3.413 a	3.323 a	3.500 a	*
NDRE[4]	0.378 bc	0.372c	0.434 a	0.419 ab	0.420 ab	*
TCARI/ OSAVI[5]	0.416 a	0.381 ab	0.344 b	0.337 b	0.253c	***
28/11/2022 (67 DAS)						
NDVI	0.874c	0.895 b	0.899 ab	0.895 b	0.907 a	***
GNDVI	4.238c	4.983 b	5.830 a	4.718 bc	4.503 bc	***
NDRE	0.457c	0.497 b	0.535 a	0.480 bc	0.464 bc	**
TCARI/ OSAVI	0.308 a	0.211 b	0.204 b	0.199 b	0.118c	***
31/01/2023 (130 DAS)						
NDVI	0.689 b	0.706 b	0.780 a	0.681 b	0.689 b	*
GNDVI	2.055 b	2.038 b	2.753 a	1.623c	1.710c	***
NDRE	0.179 a	0.177 a	0.193 a	0.124 b	0.102 b	***
TCARI/ OSAVI	0.319 ab	0.273 b	0.132c	0.388 a	0.245 b	***
12/03/2023 (170 DAS)						
NDVI	0.361c	0.405c	0.717 a	0.515 b	0.213 d	***
GNDVI	0.998 cd	1.078c	2.793 a	1.345 b	0.858 d	***
NDRE	0.024c	0.035 bc	0.244 a	0.061 b	−0.032 d	***
TCARI/ OSAVI	0.751 a	0.825 a	0.347c	0.613 b	0.854 a	***

[1]. Days After Sowing (DAS); [2]. Normalized Difference Vegetation Index (NDVI); [3]. Green Normalized Difference Vegetation Index (GNDVI); [4]. Normalized Difference Red Edge Index (NDRE); [5]. Transformed Chlorophyll Absorption in Reflectance Index (TCARI) and Optimized Soil-Adjusted Vegetation Index (OSAVI); [6]. means followed by the same letter were not significantly different (ns) at $p \leq 0.05$ according to the Fisher's least significant difference (LSD); [7]. *, **, *** and ns indicate significance at $p \leq 0.05$, 0.01, and 0.001 and non-significance at $p \leq 0.05$, respectively.

3.1.1. Structural indices: NDVI and GNDVI

The statistical analysis of data collected during the 2022–2023 period suggests the following trends. In late October 2022 (37 DAS), all five biofumigant species exhibited NDVI values exceeding 0.8, see Table 1. Differences in NDVI values were statistically significant (p-value: 0.0004, see Table 1) among species. Notably, *S. alba*, *R. sativus*, and *B. napus* showed higher NDVI values than *B. carinata* and *B. juncea*. Furthermore, *S. alba* displayed a significantly higher NDVI than *B. napus* (p-value < 0.001). For GNDVI, similar trends were observed, though with two notable differences: On the one hand, *B. napus* exhibited GNDVI values comparable to *R. sativus* and *S. alba*. On the other hand, the magnitude of differences in GNDVI values among species was greater than those observed for NDVI.

By late November 2022 (67 DAS), one month after the first measurement and coinciding with the onset of frost conditions, a key observation was that B. juncea reached NDVI values comparable to those of B. napus and R. sativus, surpassing B. carinata. Meanwhile, for GNDVI, species responses varied more substantially, with B. napus showing consistently higher values than the rest. These observations highlight GNDVI's superior ability to differentiate biofumigant Brassica species during the peak vegetative development stage.

Two months later (late January 2023, 130 DAS), after a period of frost, all species exhibited reduced NDVI and GNDVI values compared to the previous measurements. B. napus showed a clear superiority in both indices, significantly outperforming the other biofumigant species. GNDVI further distinguished among groups of species (B. carinata and B. juncea vs. R. sativus and S. alba), a differentiation not evidenced by NDVI.

Finally, on March 12, 2023 (170 DAS), following an extended and intense frost period (spanning most of February and early March, as shown in Fig. 1a), NDVI values for the biofumigant species declined further. The extent of the reduction varied across species: severe in S. alba, B. carinata, and B. juncea; moderate in R. sativus; and minimal in B. napus. It resulted in a greater differentiation among species, with four statistically distinct groups identified. For GNDVI, trends mirrored those of NDVI, but B. napus maintained its GNDVI value, demonstrating its exceptional frost tolerance. This finding is agronomically significant for continental regions in Spain where frost-prone conditions prevail, emphasizing the potential of B. napus as an intercrop in horticultural rotations.

Meanwhile, in the season 2024–2025, the collected data allow us to compare the results and to evaluate the differences and similitudes among both periods. On the one hand, data collected on December 19, 2024 (92 DAS), can be compared with those obtained on November 29, 2022 (67 DAS), considered a suitable chronological reference. The most notable difference in the NDVI analysis among the five species was that R. sativus recorded the lowest value, reflecting reduced vegetative growth. This result contrasts with its vigorous early growth observed in the 2022–2023 cycle. The difference may be related to varying weather conditions between the two years, particularly the earlier frost incidence in 2024 compared to 2022. This shift in timing could have limited the accumulation of reserves in the underground biomass, which is essential for frost tolerance in R. sativus.

Concerning the GNDVI analysis for the same date, the species were clearly divided into two groups with statistically significant differences. B. napus, S. alba, and B. juncea had higher GNDVI values than the other two species, with R. sativus again showing the lowest GNDVI rate. These results confirm the trend observed in the previous results; GNDVI provides a clearer separation among species based on vegetative development than NDVI. Despite differences in sensitivity, both indices showed comparable patterns across the five species, suggesting a stable correlation between them.

On the other hand, data collected on January 19, 2025 (123 DAS), revealed a general decline in NDVI values across all species compared to

Table 2
Vegetation indices values for biofumigant species across different sampling dates during the second cycle.

Sampling date and index	Species					
	B. carinata	*B.juncea*	*B.napus*	*R. sativus*	*S. alba*	***p value***
19/12/2024 (92 DAS[1])						
NDVI[2]	0.842bc[6]	0.857abc	0.869ab	0.822c	0.894a	*
GNDVI[3]	3.975b	4.655a	5.303a	3.358b	4.773a	***
NDRE[4]	0.301bc	0.345ab	0.356a	0.285c	0.339ab	*
TCARI/OSAVI[5]	0.007c	−0.021bc	−0.107b	0.112d	−0.306a	***
19/01/2025 (123 DAS)						
NDVI	0.726c	0.750bc	0.791ab	0.639d	0.811a	***
GNDVI	3.520b	4.068b	4.860a	2.783c	4.945a	***
NDRE	0.267bc	0.299ab	0.321a	0.238c	0.280abc	*
TCARI/OSAVI	0.190c	0.155bc	0.095b	0.272d	−0.042a	***

[1]. Days After Sowing (DAS); [2]. Normalized Difference Vegetation Index (NDVI); [3]. Green Normalized Difference Vegetation Index (GNDVI); [4]. Normalized Difference Red Edge Index (NDRE); [5]. Transformed Chlorophyll Absorption in Reflectance Index (TCARI) and Optimized Soil-Adjusted Vegetation Index (OSAVI); [6]. means followed by the same letter were not significantly different (ns) at $p \leq 0.05$ according to the Fisher's least significant difference (LSD); [7]. *, **, *** and ns indicate significance at $p \leq 0.05$, 0.01, and 0.001 and non-significance, respectively.

the previous sampling date. This reduction was particularly pronounced in *R. sativus*, which accentuated the contrast among species. Only *B. napus* and *S. alba* maintained NDVI values close to 0.8, while *R. sativus* dropped below 0.65. A similar trend was observed for GNDVI, although B. napus and S. alba either maintained or experienced only a slight decrease in their values. This stability allowed for a clearer distinction from the remaining biofumigant species, reinforcing the superior ability of GNDVI to discriminate among species during late winter stages of development.

Based on the collected data, GNDVI proved to be a more effective indicator for evaluating species performance across both growing seasons. A similar temporal pattern was observed for most species, with a general decline in GNDVI values from November to January. However, *S. alba* was an exception, exhibiting increased GNDVI values during that period. For the remaining species, the decrease in GNDVI was more pronounced in the 2022–2023 season than in 2024–2025, likely reflecting differing weather conditions between the two years. Notably, average GNDVI values in November 2024 (4.41) were lower than those recorded in November 2022 (4.85), which may be attributed to higher precipitation levels in October 2024. Increased rainfall likely resulted in cooler temperatures and reduced solar radiation, thereby limiting vegetative development. In contrast, average GNDVI values in January 2025 (4.04) remained substantially higher than those in January 2023 (2.04), indicating a less severe decline and possibly milder winter conditions in the second cycle.

Regarding NDVI, both cycles showed a consistent decline in values from November to January. In November, *B. napus* exhibited the highest NDVI values in both years. However, this trend did not persist into January, suggesting that *B. napus*'s vegetative advantage may be more sensitive to mid-winter conditions than indicated by early-season measurements.

3.1.2. Chlorophyll indices: NDRE

Regarding the 2022–2023 dataset, the statistical analysis of NDRE values across sampling dates revealed trends largely comparable to those observed for GNDVI on three occasions: late October (37 DAS), late November (67 DAS), and mid-March (170 DAS). However, a notable divergence was observed in late January 2023 (130 DAS). At this stage, while B. napus exhibited significantly higher GNDVI values than B. carinata and B. juncea, NDRE values for these three species were statistically similar (Table 1). When comparing NDRE with NDVI, the general observations made for GNDVI also apply: NDRE provided clearer differentiation among species at specific growth stages, particularly during periods of active vegetative development, thereby offering superior discriminative power compared to NDVI.

In the 2024–2025 season, NDRE values recorded on December 19, 2024 (92 DAS), followed patterns closely aligned with those of NDVI. Between December and January, a modest and uniform decrease in NDRE values was observed across all species.

Compared to the first growing season, the most striking feature was the overall lower NDRE levels across all species, a trend also observed for GNDVI. In the January, 2025 (123 DAS) sampling, statistical analysis revealed nearly identical NDRE trends for the five species, with all exhibiting similar reductions relative to the December values.

3.1.3. Combined indices: TCARI/OSAVI

During the October and November 2022 (37 and 67 DAS) samplings, the statistical analysis of this combined index for the biofumigant species revealed a well-defined pattern: the five species were grouped into three statistically distinct clusters. The first group consisted of B. carinata, which showed the highest TCARI/OSAVI values, followed by a second group comprising B. juncea, B. napus, and R. sativus. The final group included S. alba, with significantly lower TCARI/OSAVI values than the other species (Table 1).

In the January 2023 (130 DAS) sampling, notable changes were observed. *R. sativus* displayed the highest TCARI/OSAVI value, while *B. napus*, previously part of the intermediate group, exhibited the lowest value among the species. By March 2023 (170 DAS), following an extended frost period, the statistical analysis again differentiated the species into three groups. *B. carinata*, *B. juncea*, and *S. alba* formed the first group, with the highest TCARI/OSAVI values, reflecting a significant reduction in vegetative growth due to frost sensitivity. At the other extreme, *B. napus* showed the lowest TCARI/OSAVI value, even though the index increased compared to its January value. These results underscore the frost tolerance of *B. napus*, making it a promising candidate for intercropping in frost-prone regions. Finally, *R. sativus* occupied an intermediate position, with its TCARI/OSAVI value closer to the first group, driven by a greater reduction in vegetative growth relative to the decrease in chlorophyll indices. As TCARI/OSAVI is a combined index, exploring its relationships with other indices studied is of interest.

During the December 2024 sampling (92 DAS), the combined TCARI/OSAVI index grouped the five biofumigant species into four distinct clusters (Table 2). Three species—*B. juncea*, *B. napus*, and *S. alba*—showed negative TCARI/OSAVI values, with *S. alba* recording the lowest. By January 2025 (123 DAS), *R. sativus* displayed the highest value, while *S. alba* continued to show the lowest TCARI/OSAVI among the species.

Text

At both cycles, the statistical analysis of this combined index across the different biofumigant species yielded consistent results in terms of species grouping. *R. sativus* showed the highest values for this index, reflecting its lower vegetative development despite having a lower chlorophyll content (NDRE). On the contrary, *S. alba* exhibited the lowest TCARI/OSAVI values, mainly due to its greater vegetative

growth. Therefore, the results from this second year highlight, similarly to the observations from the previous year, the significant influence of the structural component (vegetative development) on this combined index.

3.1.4. Relationships between phyto-spectral indices

The robust regression curve between NDVI and GNDVI throughout both periods, as seen in Fig. 2a, highlights the consistent relationship between these vegetative development indices (R2: 0.89). Despite the strong relationship between GNDVI and NDRE, as shown in Fig. 2b, the visual analysis suggests the presence of two distinct clusters of data points. These clusters correspond to two periods in terms of frost conditions, representing a frost-free phase and the frost-affected conditions. The association between NDVI and NDRE was also strong ($R^2 = 0.84$), showing a clear relationship between these indices that remained unaffected by frost conditions (Fig. 2c).

The analysis of the relationship between TCARI/OSAVI and GNDVI (Fig. 3a), reveals that, comparatively, this relationship was less consistent than with NDVI in individual analyses for the late November and late January sampling dates. Nevertheless, it became more consistent in the mid-March analysis. On the contrary, as shown in Fig. 3b, the global NDRE and TCARI/OSAVI analysis shows a slightly lower degree of agreement overall. Specifically, the strength of the association decreased during the late November and late January sampling dates, resulting in reduced consistency in the global analysis combining all sampling dates.

The relationship between NDVI and TCARI/OSAVI (Fig. 3c) was highly consistent in the global analysis combining all six dates. This consistency underscores the strong influence of the structural component (vegetative growth and development) on the combined TCARI/OSAVI index.

In summary, as illustrated in Fig. 3, the relationship between these indices weakens during the growth stages when species reach their maximum vegetative development, characterized by high GNDVI/NDRE values and low TCARI/OSAVI values.

3.2. Correlations between phyto-spectral indices and above-ground dry biomass and glucosinolate concentration

A detailed analysis of biomass production, GSLs concentration, and profiles of biofumigant species on the two sampling dates is available in our previous publication (Arroyo et al., 2025). This study focuses on analyzing the relationships between these parameters, which are key to biofumigation, and the phyto-spectral indices determined via remote sensing. These relationships between above-ground biomass (AGB) and glucosinolates (GSLs) content—both as the concentration in the plant material and per unit of crop surface—are of practical relevance for the large-scale implementation of this technique, and their corresponding coefficients of determination (R^2) with each of the four phyto-spectral indices measured on two sampling dates are summarized in Table 3 for both studied periods. In addition, considering the considerable

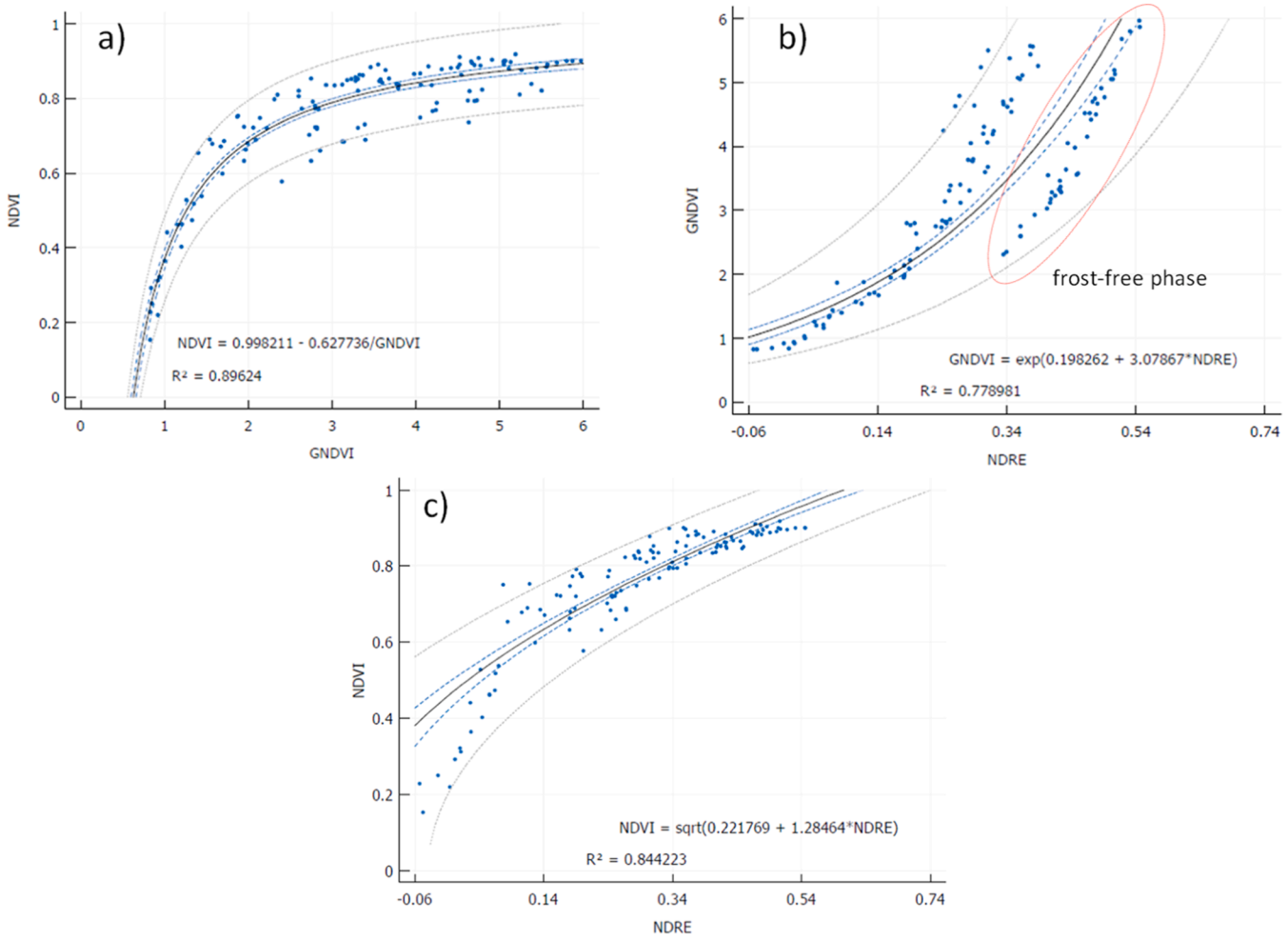

Fig. 2. Analysis of the relationship between a) Normalized Difference Vegetation Index (NDVI) and Green Normalized Difference Vegetation Index (GNDVI), b) Green Normalized Difference Vegetation Index (GNDVI) and Normalized Difference Red Edge Index (NDRE), and c) NDVI and TCARI/OSAVI. R^2 expressed the regression coefficient. Blue dots represent observed values. The solid black line corresponds to the fitted regression model. Dashed blue lines indicate the 95 % confidence interval for the mean response, while dashed grey lines represent the 95 % prediction interval for new observations.

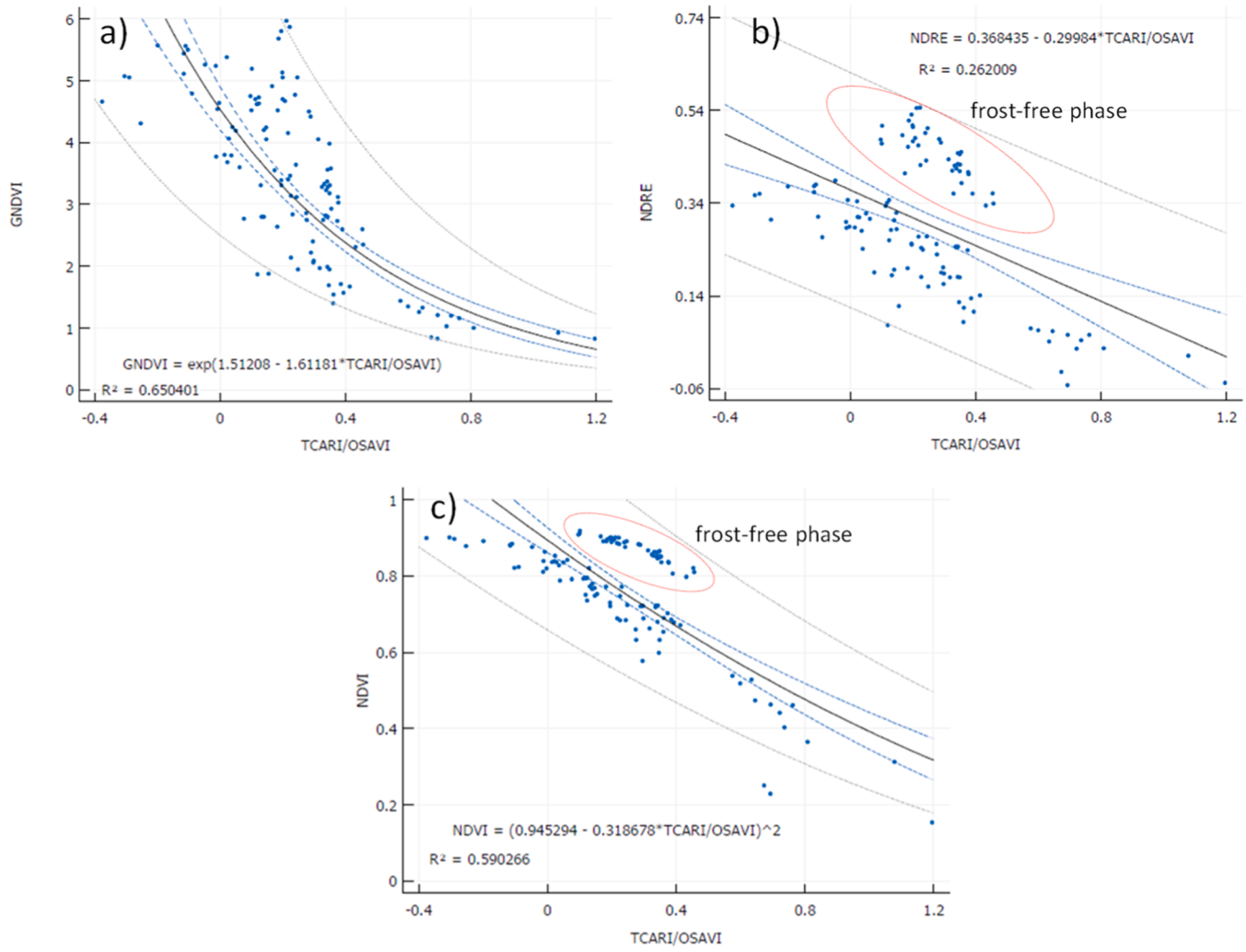

Fig. 3. Analysis of the relationship between Green Normalized Difference Vegetation Index (GNDVI) and TCARI/OSAVI (a) and Normalized Difference Red Edge Index (NDRE) and Transformed Chlorophyll Absorption Ratio Index/Optimized Soil Adjusted Vegetation Index (TCARI/OSAVI) (b) for biofumigant species during the 2022–2023 cycle. R^2 expressed the regression coefficient. Blue dots represent observed values. The solid black line corresponds to the fitted regression model. Dashed blue lines indicate the 95 % confidence interval for the mean response, while dashed grey lines represent the 95 % prediction interval for new observations.

Table 3
Coefficients of determination (R^2) for relationships between total above-ground dry biomass, glucosinolate concentration and glucosinolate content incorporated into the soil with phyto-spectral indices.

Year	Parameters	AGB[1] (g dry matter/m²)		GSLs[2] (μmol/g dry matter)		GSLs (μmol/m²)	
	Sampling date and index	31/01/2023 (130 DAS[3])	12/03/2023 (170 DAS)	31/01/2023 (130 DAS)	12/03/2023 (170 DAS)	31/01/2023 (130 DAS)	12/03/2023 (170 DAS)
2022-2023	NDVI[4]	0.03 ns[8]	0.80 **	0.04 ns	0.35 ns	0.08 ns	0.19 ns
	GNDVI[5]	0.04 ns	0.85 **	0.58 *	0.46 *	0.45 *	0.22 ns
	NDRE[6]	0.10 ns	0.86 **	0.58 *	0.41 *	0.66 *	0.19 ns
	TCARI/OSAVI[7]	0.04 ns	0.78 **	0.63 *	0.50	0.61 *	0.22 ns
	Sampling date and index	19/12/2024 (92 DAS)	19/01/2025 (123 DAS)	19/12/2024 (92 DAS[3])	19/01/2025 (123 DAS)	19/12/2024 (92 DAS[3])	19/01/2025 (123 DAS)
2024-2025	NDVI	0.36 *	0.62 ***	0.08 ns	0.07 ns	0.02 ns	0.02 ns
	GNDVI	0.05 ns	0.41 **	0.05 ns	0.03 ns	0.06 ns	0.03 ns
	NDRE	0.19 ns	0.52 ***	0.10 ns	0.02 ns	0.09 ns	0.03 ns
	TCARI/OSAVI	0.52 ***	0.52 ***	0.06 ns	0.06 ns	0.00 ns	0.00 ns

[1.] Total Above-ground Dry Biomass (AGB); [2.] Glucosinolates (GSLs); [3.] Days After Sowing (DAS); [4.] Normalized Difference Vegetation Index (NDVI); [5.] Green Normalized Difference Vegetation Index (GNDVI); [6.] Normalized Difference Red Edge Index (NDRE); [7.] Transformed Chlorophyll Absorption in Reflectance Index (TCARI) and Optimized Soil-Adjusted Vegetation Index (OSAVI); [8.] *, **, *** and ns indicate significance at $p \leq 0.05$, 0.01, and 0.001 and non-significance at $p \leq 0.05$, respectively. Differences in significance notation between years reflect the unequal number of flights and data points (2022–2023: four; 2024–2025: two), which altered the degrees of freedom.

Table 4
Coefficients of determination (R^2) for relationships between total above-ground dry biomass, glucosinolate concentration and glucosinolate content incorporated into the soil with phyto-spectral indices.

Parameters	AGB[1]			GSLs[2]			GSLs		
	(g dry matter/m²)			(μmol/g dry matter)			(μmol/m²)		
Sampling date and index	SR[7]	MR[8]	RL[9]	SR	MR	RL	SR	MR	RL
NDVI[3]	0.13***[10]	-	0.28 (0.47)	0.14***	-	0.63 (0.84)	0.07*	-	0.15 (0.54)
GNDVI[4]	0.26***	-	0.61 (0.69)	0.23***	-	0.68 (0.61)	0.15**	-	0.13 (0.42)
NDRE[5]	0.22***	-	0.58 (0.59)	0.22***	-	0.68 (0.87)	0.08*	-	0.54 (0.77)
TCARI/OSAVI[6]	0.20***	-	0.53 (0.60)	0.21***	-	0.42 (0.70)	0.10*	-	0.21 (0.31)
All	-	0.34***	0.58 (0.81)	-	0.20 ns	0.32 (0.50)	-	0.13 ns	0.36 (0.75)

[1.] Total Above-ground Dry Biomass (AGB); [2.] Glucosinolates (GSLs); [3.] Normalized Difference Vegetation Index (NDVI); [4.] Green Normalized Difference Vegetation Index (GNDVI); [5.] Normalized Difference Red Edge Index (NDRE); [6.] Transformed Chlorophyll Absorption in Reflectance Index (TCARI) and Optimized Soil-Adjusted Vegetation Index (OSAVI); [7.] Simple Regression (SR); [8.]Multiple Regression (MR); [9] Regression Learner (RL);. [10.] *, **, *** and ns indicate significance at $p \leq 0.05$, 0.01, and 0.001 and non-significance at $p \leq 0.05$, respectively. Data between brackets indicate the R^2 values for the test dataset.

variability of results in the second periods when data is analysed for different DAS, in Table 4 we present the relationships for the whole period. In this table, the results obtained with the three used approaches (Simple Regression (SR), Multiple Regression (MR), and Regression Learner (RL)) are summarized.

3.2.1. *Relationships between phyto-spectral indices and Above-ground Dry Biomass (AGB)*

Although the analyses performed separately for each growing cycle showed strong relationships between AGB and the various spectral indices, the regression coefficients did not exceed 0.3 when data from both cycles were analyzed together. This reduction in relationship strength may be attributed to the contrasting climatic conditions between the two periods, particularly in terms of temperature and precipitation regimes. Similarly, multiple regression analysis did not result in a substantial improvement in the overall predictive power of the models.

However, the analysis performed using Regression Learner (RL) tool showed a notable improvement in model consistency, see values in RL column of Table 4 for AGB. In particular, GNDVI achieved R^2 values of 0.61 for the training set and 0.69 for the test set. NDRE and TCARI/OSAVI yielded slightly lower performance, while NDVI showed significantly lower R^2 values in both subsets. Finally, combining all indices into a single model did not lead to any substantial improvement in predictive accuracy (Fig. 4).

3.2.2. *Relationship between glucosinolate concentrations and quantities of GSLs in above-ground dry biomass with phyto-spectral indices*

Experimental results reveal that the relationships between phyto-spectral indices and both glucosinolates (GSLs) concentrations and quantities in above-ground dry biomass (AGB) vary depending on the sampling date (Table 3).

The considerations previously discussed for the relationship between AGB and phyto-spectral indices also apply here: very low R^2 values were observed for all indices when estimating GSLs concentration. Similarly, the application of Regression Learner (RL) analysis improved estimation accuracy, with R^2 values approaching 0.7. In this case, NDRE yielded the highest R^2 values among the indices evaluated.

Finally, when considering the total amount of glucosinolates incorporated into the soil per square meter—a parameter that integrates both GSLs concentration and biomass production—the results closely resembled those obtained for GSLs concentration alone. This indicates that, for total GSLs input, variation in GSLs concentration plays a more decisive role than variation in biomass. Once again, NDRE emerged as the most reliable predictor of this integrated parameter.

Fig. 4 displays the observed versus predicted values obtained using the three analytical methodologies applied for the prediction of above-ground biomass, GSLs concentration, and total GSLs input per square meter.

The comparison includes results from Simple Regression (SR), Multiple Regression (MR), and machine learning-based models generated using Regression Learner (RL). As shown in the figure, the use of RL clearly enhanced predictive performance across all three parameters, yielding more accurate and consistent estimations than traditional regression approaches. This improvement is evident in the tighter clustering of data points around the 1:1 line and in the higher R^2 values obtained.

4. Conclusions

The dependence on chemical fumigants for soil disinfection poses significant environmental challenges. Many of these products, such as 1,3-dichloropropene and chloropicrin, have been banned or severely restricted in the European Union due to their harmful environmental effects and potential health risks (Commission of the European Communities. 2022a,b). This regulatory shift limits the availability of conventional soil disinfection methods and urges the adoption of more sustainable alternatives. In contrast, biofumigation, based on the use of plant species that produce GSLs, emerges as an effective and environmentally friendly approach. Although various species have demonstrated their ability to accumulate GSLs (Agerbirk and Olsen, 2012; Fahey et al., 2001; Gimsing and Kirkegaard, 2009; Morris et al., 2020; Wieczorek et al., 2024), originating biocidal isothiocyanates, the lack of knowledge regarding the optimal incorporation timing, the exact amount of accumulated GSLs, and the scarce availability of accessible and cost-effective evaluation tools limit farmers' ability to make informed technical decisions.

The analysis of the relationships between phyto-spectral indices and biofumigant characteristics reveals distinct patterns of utility for each index. GNDVI, NDRE, and TCARI/OSAVI demonstrate broader applicability. These indices not only share NDVI's ability to estimate biomass but also excel in providing approximate estimations of GSLs concentrations and quantities in the AGB of biofumigant species. Among them, NDRE stands out as particularly effective, especially during the stages of peak vegetative growth. This enhanced ability underscores these indices' potential as practical tools for supporting decision-making in biofumigation practices, facilitating the timing and management of species incorporation into the soil for maximum effectiveness. In contrast, NDVI emerges as a limited tool, effective primarily for detecting differences in biomass among biofumigant species when significant variations in vegetative growth occur. However, its role as an estimator for GSLs concentration or total GSLs content per crop surface is negligible, making it less suitable for applications beyond biomass differentiation.

Moreover, beyond improved accuracy, these tools can be applied throughout the crop's growth period, regardless of the days after sowing (DAS), reducing the need for multiple models and avoiding redundancy—one of the main limitations of traditional regression approaches. This is particularly useful for companies offering drone-based treatments, which require a single, reliable model for consistent application across different crop stages. In future research, we aim to optimize crop

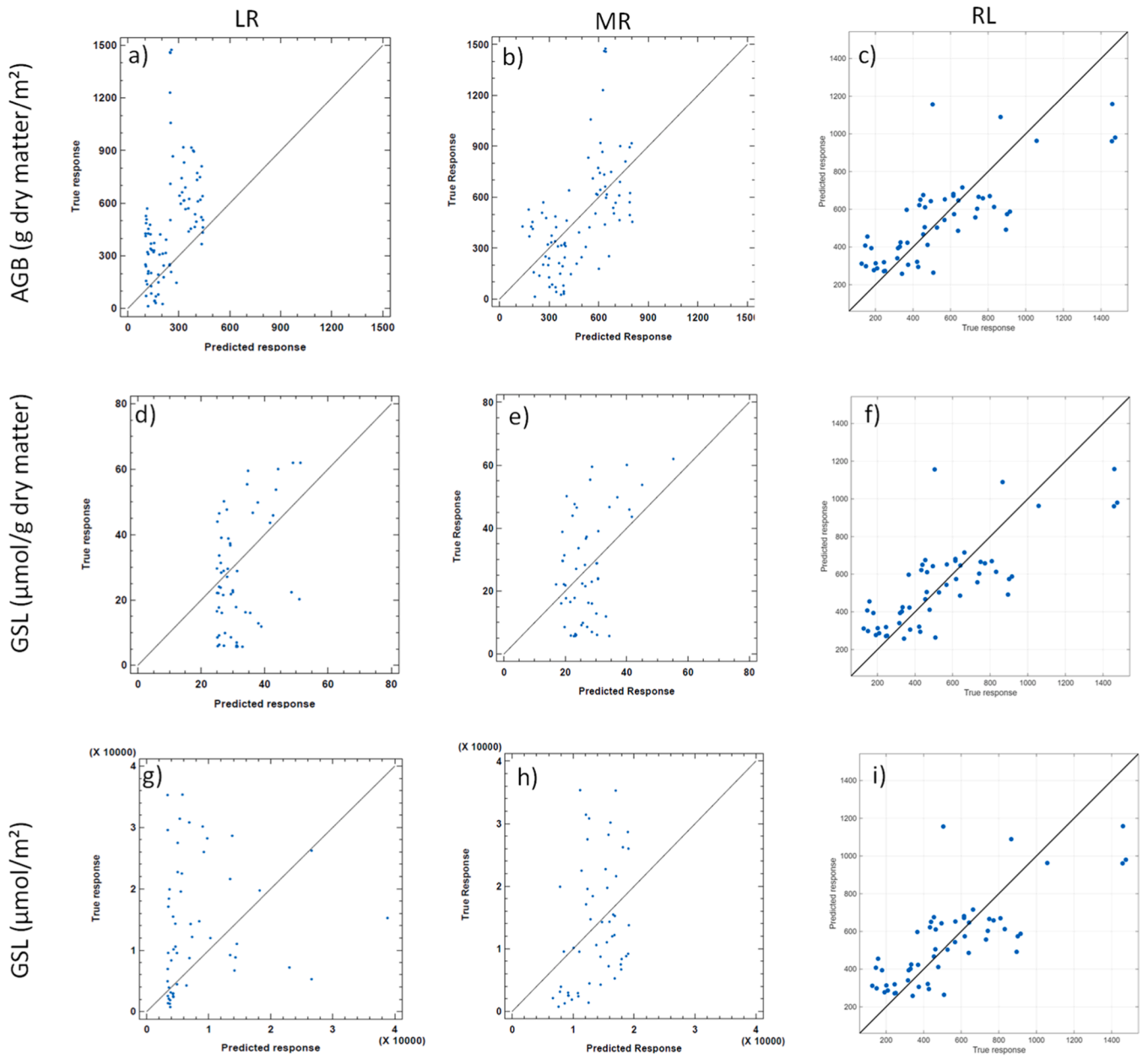

Fig. 4. Observed vs. predicted values for three key variables: above-ground dry biomass (AGB) (top row), glucosinolate concentration (middle row), and total glucosinolate content per square meter (bottom row), using different modeling approaches. Left column (a, d, g): simple linear regression (LR) using GNDVI; center column (b, e, h): multiple linear regression (MR) incorporating all vegetation indices and species code; right column (c, f, i): regression learner models (RL) using the most relevant index (GNDVI for AGB, NDRE for GSLs parameters) and species code. Blue dots represent observed values; the solid black line indicates the identity line (perfect prediction, y = x).

management strategies to enhance GSLs production and strengthen the aliphatic GSL profile to improve its effectiveness against specific soil-borne pathogens and nematodes. Additionally, the potential of these crops as CO_2 and nitrogen sequestrators should be further explored to assess their environmental benefits. Investigating their role in both mitigating climate change and improving soil quality will provide valuable insights into their broader agroecological potential.

Funding

This research was funded by the Plan Estatal de Investigación Científica, Técnica y de Innovación 2021–2023 and Proyectos de Generación de Conocimiento, Convocatoria 2021 (PID2021–125545OR-C22).

CRediT authorship contribution statement

Daniel Palmero: Writing – review & editing, Project administration, Investigation, Funding acquisition, Conceptualization. **Lorena Parra:** Writing – original draft, Software, Data curation. **Rubén Linares:** Writing – original draft, Validation, Resources, Methodology. **Jose Soler:** Methodology. **Arroyo Juan:** Writing – original draft, Visualization, Validation, Supervision, Investigation, Data curation, Conceptualization.

Declaration of Competing Interest

Daniel Palmero reports financial support was provided by National Plan for Scientific and Technical Research and Innovation. Daniel

Palmero reports a relationship with Plan Estatal de Investigación Científica, Técnica y de Innovación that includes: funding grants. If there are other authors, they declare that they have no known competing financial interests or personal relationships that could have appeared to influence the work reported in this paper.

Data availability

The datasets supporting this study are openly available in e-cienciaDatos at: http://doi.org/10.21950/0UHHSU.

References

Agerbirk, N., Olsen, C.E., 2012. Glucosinolate structures in evolution. Phytochemistry 77, 16–45. https://doi.org/10.1016/j.phytochem.2012.02.005.

Arroyo, J.M., Soler, J., Linares, R., Palmero, D., 2025. Strategies for selecting potentially effective biofumigant species for optimal biofumigation outcomes. Agriculture 15 (2), 147. https://doi.org/10.3390/agriculture15020147.

Bellostas, N., Sørensen, J.C., Sørensen, H., 2004. Qualitative and quantitative evaluation of glucosinolates in cruciferous plants during their life cycles. Agroindustria 3 (3), 5–10. ⟨http://orgprints.org/5611⟩.

Bellostas, N., Sørensen, J.C., Sørensen, H., 2007. Profiling glucosinolates in vegetative and reproductive tissues of four brassica species of the U-triangle for their biofumigation potential. J. Sci. Food Agric. 87 (8), 1586–1594. https://doi.org/10.1002/jsfa.2896.

Ben Ammar, H., Arena, D., Treccarichi, S., Di Bella, M.C., Marghali, S., Ficcadenti, N., Lo Scalzo, R., Branca, F., 2023. The effect of water stress on the glucosinolate content and profile: a comparative study on roots and leaves of brassica oleracea L. Crops. Agronomy 13 (2). https://doi.org/10.3390/agronomy13020579.

Björkman, M., Klingen, I., Birch, A.N.E., Bones, A.M., Bruce, T.J.A., Johansen, T.J., Meadow, R., Mølmann, J., Seljåsen, R., Smart, L.E., Stewart, D., 2011. Phytochemicals of brassicaceae in plant protection and human health - influences of climate, environment and agronomic practice. Phytochemistry 72 (7), 538–556. https://doi.org/10.1016/j.phytochem.2011.01.014.

Brant, V., Pivec, J., Fuksa, P., Neckář, K., Kocourková, D., Venclová, V., 2011. Biomass and energy production of catch crops in areas with deficiency of precipitation during summer period in central bohemia. Biomass.. Bioenergy 35 (3), 1286–1294. https://doi.org/10.1016/j.biombioe.2010.12.034.

Brennan, R.J. B., Glaze-Corcoran, S., Wick, R., & Hashemi, M., 2020. Biofumigation: An alternative strategy for the control of plant parasitic nematodes. J. Integr. Agric. (Vol. 19, Issue 7, pp. 1680–1690). Chinese Academy of Agricultural Sciences. https://doi.org/10.1016/S2095-3119(19)62817-0.

Chowdhury, M., Ngo, V.-D., Islam, N., Ali, M., Islam, S., Rasool, K., Park, S.-U., Chung, S.-O., 2021. Estimation of glucosinolates and anthocyanins in kale leaves grown in a plant factory using spectral reflectance. Horticulturae 7 (3), 56. https://doi.org/10.3390/horticulturae7030056.

Clarkson, J., Michel, V., Neilson, R., 2015. Soil borne disease focus group. Biofumigation Control Soil. Dis. ⟨https://ec.europa.eu/eip/agriculture/sites/default/files/9_eip_sbd_mp_biofumigation_final_0.pdf⟩.

Commission of the European Communities, 2022a. Commission implementing regulation (EU) 2022/751 of May 16 2022 concerning the non-approval of the active substance chloropicrin, in accordance with regulation (EC) no 1107/2009 of the european parliament and of the council concerning the placing of plant protection products on the market. Off. J. Eur. Union 7–9. ⟨https://eur-lex.europa.eu/eli/reg_impl/2022/751/oj⟩. L 136, 17.5.2022.

Commission of the European Communities, 2022b. Commission implementing regulation (EU) 2022/740 of May 13 2022 concerning the non-approval of the active substance 1,3-dichloropropene, in accordance with regulation (EC) no 1107/2009 of the european parliament and of the council concerning the placing of plant protection products on the market. Off. J. Eur. Union 30–32. ⟨https://eur-lex.europa.eu/eli/reg_impl/2022/740/oj⟩. L 134, 16.5.2022.

Elhakeem, A., van der Werf, W., Bastiaans, L., 2021. Radiation interception and radiation use efficiency in mixtures of winter cover crops. Field Crops Res. 264, 1–9. https://doi.org/10.1016/j.fcr.2020.108034.

Fahey, J.W., Zalcmann, A.T., Talalay, P., 2001. The chemical diversity and distribution of glucosinolates and isothiocyanates among plants. Phytochemistry 56, 5–51. https://doi.org/10.1016/S0031-9422(00)00316-2.

Fourie, H., Ahuja, P., Lammers, J., Daneel, M., 2016. Brassicacea-based management strategies as an alternative to combat nematode pests: a synopsis. Crop Prot. 80, 21–41. https://doi.org/10.1016/j.cropro.2015.10.026.

Gabbrielli, M., Corti, M., Perfetto, M., Fassa, V., Bechini, L., 2022. Satellite-Based frost damage detection in support of winter cover crops management: a case study on White mustard. Agronomy 12 (9). https://doi.org/10.3390/agronomy12092025.

Gimsing, A.L., Kirkegaard, J.A., 2009. Glucosinolates and biofumigation: fate of glucosinolates and their hydrolysis products in soil. Phytochem. Rev. 8 (1), 299–310. https://doi.org/10.1007/s11101-008-9105-5.

Gitelson, A.A., Kaufman, Y.J., Merzlyak, M.N., Blaustein, J., 1995. Use of a Green channel in remote sensing of global vegetation from EOS-MODIS. Remote Sens. Environ. 58 (3), 289–298. https://doi.org/10.1016/S0034-4257(96)00072-7.

Haboudane, D., Miller, J.R., Tremblay, N., Zarco-Tejada, P.J., Dextraze, L., 2002. Integrated narrow-band vegetation indices for prediction of crop chlorophyll content for application to precision agriculture. Remote Sens. Environ. 81 (2-3), 416–426. https://doi.org/10.1016/S0034-4257(02)00018-4.

Haramoto, E.R., Gallandt, E.R., 2004. Brassica cover cropping for weed management: a review. Renew. Agric. Food Syst. 19 (04), 187–198. https://doi.org/10.1079/RAFS200490.

ISO 9167-1, 1992. Part 1: method using high-performance liquid chromatography. In rapeseed -Determination of glucosinolates content. Tech. Comm. ISO/TC 34/SC 2.

Kirkegaard, J.A., Sarwar, M., 1998. Biofumigation potential of brassicas I. Variation in glucosinolate profiles of diverse field-grown brassicas. Plant Soil 201, 71–89. https://doi.org/10.1023/A:1004364713152.

Kirkegaard, J.A., Gardner, P.A., Desmarchelier, J.M., Angus, J.F., 1993. Biofumigation - using brassica species to control pests and diseases in horticulture and agriculture. In: Wratten, N., Mailer, R.J. (Eds.), Agricultural Research Institute. N.S.W. 9th Australian Research Assembly on Brassicas, Wagga Wagga, pp. 77–82.

Liu, Y., Liu, S., Li, J., Guo, X., Wang, S., Lu, J., 2019. Estimating biomass of winter oilseed rape using vegetation indices and texture metrics derived from UAV multispectral images. Comput. Electron. Agric. 166. https://doi.org/10.1016/j.compag.2019.105026.

Lukas, V., Huňady, I., Kintl, A., Mezera, J., Hammerschmiedt, T., Sobotková, J., Brtnický, M., Elbl, J., 2022. Using UAV to identify the optimal vegetation index for yield prediction of oil seed rape (*brassica napus* L.) at the flowering stage. Remote Sens 14 (19). https://doi.org/10.3390/rs14194953.

Matthiessen, J., Kirkegaard, J., 2006. Biofumigation and enhanced biodegradation: opportunity and challenge in soilborne pest and disease management. Crit. Rev. Plant Sci. 25 (3), 235–265. https://doi.org/10.1080/07352680600611543.

Mawlong, I., Sujith Kumar, M.S., Gurung, B., Singh, K.H., Singh, D., 2017. A simple spectrophotometric method for estimating total glucosinolates in mustard de-oiled cake. Int. J. Food Prop. 20 (12), 3274–3281. https://doi.org/10.1080/10942912.2017.1286353.

Morris, E.K., Fletcher, R., Veresoglou, S.D., 2020. Effective methods of biofumigation: a meta-analysis. Plant Soil 446 (1–2), 379–392. https://doi.org/10.1007/s11104-019-04352-y.

Ngo, V.D., Jang, B.E., Park, S.U., Kim, S.J., Kim, Y.J., Chung, S.O., 2019. Estimation of functional components of Chinese cabbage leaves grown in a plant factory using diffuse reflectance spectroscopy. J. Sci. Food Agric. 99 (2), 711–718. https://doi.org/10.1002/jsfa.9237.

Rondeaux, G., Steven, M., Baret, F., 1996. Optimization of Soil-Adjusted vegetation indices. Remote Sens. Environ. 55 (2), 95–107. https://doi.org/10.1016/0034-4257(95)00186-7.

Rouse, J.W., Haas, R.H., Scheel, J.A., & Deering, D.W., 1974. Monitoring vegetation systems in the great plains with ERTS. In Proceedings, 3rd Earth Resource Technology Satellite (ERTS) Symposium. NASA. Goddard Space Flight Center. Maryland. 48–62. https://ntrs.nasa.gov/api/citations/19740022614/downloads/19740022614.pdf.

dos Santos, C.A., de Souza, A.C., Ferreira, M.G., 2021. Biofumigation with species of the *brassicaceae* family: a review. Cienc. Rural 51 (1), 1–17. https://doi.org/10.1590/0103-8478cr2020040.

Sarwar, M., Kirkegaard, J.A., 1998. Biofumigation potential of brassicas II. Effect of environment and ontogeny on glucosinolate production and implications for screening. Plant Soil 201, 91–101. ⟨https://www.jstor.org/stable/42948308⟩.

Soengas, P., Madloo, P., Lema, M., 2023. Spectral reflectance indexes reveal differences in the physiological status of *brassica oleracea* with contrasting glucosinolate content under biotic stress. Plants 12 (14). https://doi.org/10.3390/plants12142698.

Tucker, C.J., 1979. Red and photographic infrared linear combinations for monitoring vegetation. Remote Sens. Environ. 8, 127–150. https://doi.org/10.1016/0034-4257(79)90013-0.

Wieczorek, R., Zydlik, Z., Zydlik, P., 2024. Biofumigation treatment using *tagetes patula*, *sinapis alba* and *raphanus sativus* changes the biological properties of replanted soil in a fruit tree nursery. Agriculture 14 (7). https://doi.org/10.3390/agriculture14071023.

Zamani-Noor, N., Feistkorn, D., 2022. Monitoring growth status of winter oilseed rape by NDVI and NDYI derived from UAV-based red–green–blue imagery. Agronomy 12 (9). https://doi.org/10.3390/agronomy12092212.